Tensile –shear response correlation of ultra-high-performance fiber-reinforced concrete at high strain rates

Tri Thuong Ngo[1*], Cong Bang Phan[2]

Abstract: The superior mechanical characteristics of ultra-high-performance fiber-reinforced concrete (UHPFRC) hold great potential for application in structures subjected to extreme loads, such as impacts or blasts. However, the practical application of this material in engineering is limited due to a lack of information about its mechanical properties, especially at high strain rates. In this study, the shear behavior of UHPFRC was investigated using a novel shear test setup installed in the universal testing machine (UTM) for static tests and the improved-strain energy frame impact machine (I-SEFIM) for high strain rate tests, respectively. Additionally, effect of fiber volume contents and the correlation between shear and tensile behavior were also clarified. The experimental results indicated a significant increase in the shear strength of UHPFRC as the fiber volume content and applied strain rates increased, even though the shear strain rate sensitivity was not as high as the tensile strain rate sensitivity. The shear-tensile ratios were approximately 1.45, 0.67, and 0.66 at average strain rates 0.000667, 99, and 184 s^{-1}, respectively.

Keywords: UHPFRCs, shear resistance, tensile resistance, high-strain rates.

1. Introduction

The superior strength and energy absorption capacity of ultra-high-performance fiber-reinforced concretes (UHPFRCs) is expected to greatly improve the resistance of civil infrastructure under impacts or blasts (N. T. Tran et al., 2016), such as concrete walls under single missile attacks. Under these extreme loads, complex failure modes, including compressive, tensile, and shear failure as well as local spalling on the surface of the structure have frequently been reported (Micallef et al., 2014).

In recent years, the compressive, tensile, and flexural responses of UHPFRCs at high strain rates have been intensively investigated by a considerable number of researchers. (Wu et al., 2017) investigated the compressive strength of UHPFRC at static and high strain rates using the Hopkinson press bar (SHPB) testing, and they reported that the dynamic compressive properties increased gradually with the increase of the strain rate. (Park et al., 2016a) and (Millon et al., 2009) investigated the tensile resistance of UHPFRC at different strain rates using the different impact systems: improved-strain energy frame impact machine (I-SEFIM) and the split Hopkinson press bar, respectively. They reported that the tensile resistance of UHPFRC significantly increased with the increase of loading rates and the enhancement strongly depended on the fiber parameters such as fiber volume content, fiber type, and fiber aspect ratio. The tensile strength of UHPFRCs at high strain rates (90 to 200 s^{-1}) was reported to be 2.9 times higher than that at the static rates (Park et al., 2016b).

However, there has been still limited information on the shear resistance of UHPFRC at high strain rates, which was a dominant failure mode of structures during the impact or

[1]Fuculty of Civil Engineering, Thuyloi University
[2]Department of Transport, HCM City
[*] Corresponding author; Email: trithuong@tlu.edu.vn
Received 18th Oct. 2023
Accepted 3rd Nov. 2023
Available online 31st Dec. 2023

blast load. (Millard et al., 2010) investigated the shear resistance of UHPFRC using a drop-hammer system and reported that there was no significant strain rate dependence on shear resistance in the case of drop-hammer loading. (Ngo et al., 2019) investigated the shear resistance of UHPFRCs at high strain rates using a new shear test method installed in the developed I-SEFIM. They reported that the UHPFRC reinforced with smooth steel fiber exhibited high rate sensitivity. However, they have just investigated the shear resistance of UHPFRCs reinforced with the smooth steel fiber and up to 1.5% fiber volume fractions. In addition, the correlation between tensile, flexural, and shear resistance of UHPFRC has not been considered, this is really the gap information since the complex failure modes, including compressive, tensile, shear failure as well as local spalling on the surface of the structure have frequently been reported when infrastructure was subjected to high rate loads (Millard et al., 2010; Thai & Kim, 2014).

This study aims to understand the shear resistance as well as the correlation between shear and tensile resistance of UHPFRCs at high strain rates. The shear test method, newly developed by (Ngo et al., 2017), was used to investigate the shear resistance of UHPFRC at both static and high strain rates while their tensile resistance was investigated in a prior study (Park et al., 2016b) .

2. Experimental program

An experimental layout was designed to investigate the shear strain-rate dependent as well as shear-tensile correlation of UHPFRCs reinforced with smooth steel fiber, under static and high strain rates, as shown in Fig. 1. Three series with 18 prism shear specimen (50 x 50 x 210 mm3) of UHPFRC reinforced with 2.0 vol.-% smooth steel fiber was prepared and tested. The tensile response was investigated by (Park et al., 2016b).

2.1. Material and specimen preparation

The composition of the ultra-high-performance concrete (UHPC) matrix was shown in Table 1. The compositions by weight ratio of ingredients are 0.25, 1.10, 0.30, 0.067, and 0.2 for cement (Type I), silica fume, silica sand, silica powder, super-plasticizer, and water, respectively. Cement (Type I) satisfying Korea Standard (KS) L5201 and ASTM C150, silica fume certified by KS F2567 and ASTM C1240, the silica sand with a median grain size of 0.15 mm, and a polycarboxylate-based superplasticizer with 25% solid content by weight were used for the mixtures. The chemical compositions, physical properties, and images of compendious material were shown in Table 2 and Fig. 2, respectively, while the properties of steel fibers were listed in Table 3.

A Hobart type laboratory mixer with a controllable rotation speed and a 20-L capacity was used to prepare the UHPC mixture. The ingredients were dry mixed until the mixture showed a good distribution, then the water and super-plasticizer were gradually added while the mixing kept rotating. The fibers were sprayed by hand after checking the workability and viscosity of the mixture. The detailed procedure of mixing and curing can be found in (J.J. Park, S.T. Kang, K.T. Koh, n.d.). In their experiment, the average compressive strength of 50 mm cubic UHPC specimens was 180 MPa.

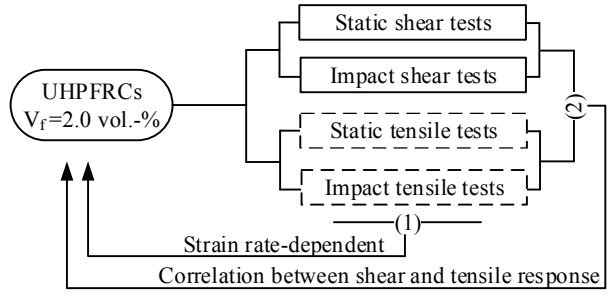

Fig 1. Experimental layout

The shear prism specimens (50 x 50 x 210 mm^3) were cast by pouring the mixture into the

mold using a scoop without any vibration. The cast specimens were covered using a plastic sheet for preventing the moisture loss, and they were stored at room temperature for 24 hours before demolding. The early age specimens were cured in a hot 90 ± 2°C water tank for 48 hours and keep drying until the ages of 28 days for testing.

Table 1. Matrix composition by weight ratio

Cement (Type I)	Silica Fume	Sand	Silica powder	Super-plasticize	Water
1.00	0.25	1.10	0.30	0.067	0.2

Table 2. Chemical composition and physical properties of cementitious materials

Chemical composition and physical properties		Cement (Type I)	Silica fume	Silica powder
Chemical composition (%)	CaO	60.6	0.27	0.20
	SiO_2	23.0	95.0	97.2
	Al_2O_3	3.41	0.0	0.0
	Fe_2O_3	3.13	0.31	0.23
	MgO	3.68	0.64	0.31
	TiO_2	0.00	0.67	0.77
	MnO	0.08	0.15	0.13
	L.O.I	2.24	2.19	0.91
Physical properties	Mean particle size (μm)	16.1	0.30	3.92
	Density (g/cc)	3.15	2.30	2.65

Table 3. Properties of steel fiber

Dimension/Length, mm	Density, ρ (g/cc)	Tensile strength, σ_u (MPa)	Elastic modulus, E (GPa)
30/0.3	7.90	2580	200

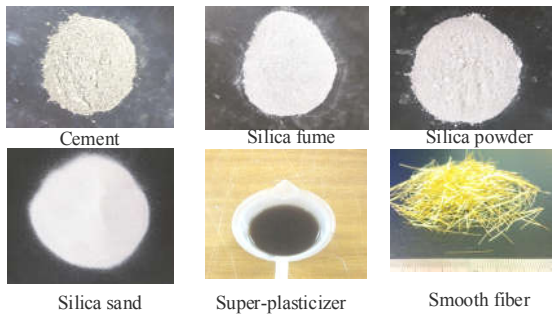

Fig 2. Images of compendious material

2.2. Test setup and procedure

Fig. 3 shows the shear test setup at static rates. The shear test setup recently proposed by (Ngo et al., 2017) was installed in the Universal Test Machine (UTM). Two ends of specimens were fixed while the load was applied on two 60 mm separated points. The shear span (*a*-horizontal distance between the inner edge of the supporting block and out the edge of the loading block) was 25 mm, yielding the span-to-depth ratios (*a/d*) was equal to 0.5. The test setup was installed in the universal test machine (UTM) with a displacement control model of 1 mm/min. The applied load was measured by a load cell installed inside the UTM and the displacement of the middle part of the specimen was measured by two linear variable differential transformers (LDVTs) attached by an aluminum frame.

Fig. 4 shows the shear test setup at high strain rates. A test setup with specimen size and boundary condition was the same as the static shear test setup, which was designed and installed in the I-SEFIM to implement shear dynamic tests. A fundamental principle of I-SEFIM was using the strain energy stored in a high-strength steel frame to generate a high-speed loading on the specimen. Firstly, a hydraulic jack stressed the coupler until the yield limit, the coupler was suddenly broken and all the strain energy stored in the high strength frame was released, leading to the entire frame and the grips moving with very high energy for breaking the specimens to the opposite side. The applied loading was measured by two dynamic strain gauges attached to the surface of the transmitter bar while the displacement was measured by a high-speed camera system. During the test, the camera captured the movement of marked points on the surfaces of the moving grip and fixed grips, with the support of high intensive light. The stress signal and displacement history were recorded by a data acquisition connecting to a computer system. Detail of test processing could be referred to (Park et al., 2016a; T. K. Tran & Kim, 2012).

The speed of the impact system could be controlled by using different coupler and energy frames (Park et al., 2016a). In this study, two combinations of coupler and energy frame were used in the setup: 1) a 800 kN capacity coupler and high strength steel energy frame; and, 2) a 400 kN capacity coupler and titanium energy frame. The theoretical impact velocity is estimated as 13.8 and 13.1 m/s by using Eq. (1) corresponding to the above combinations, respectively.

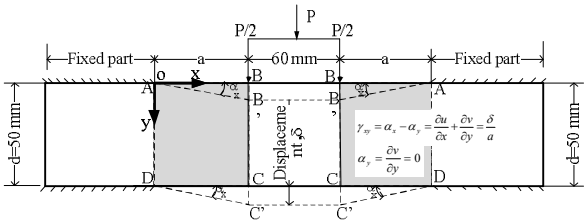

a) Scheme of shear test setup

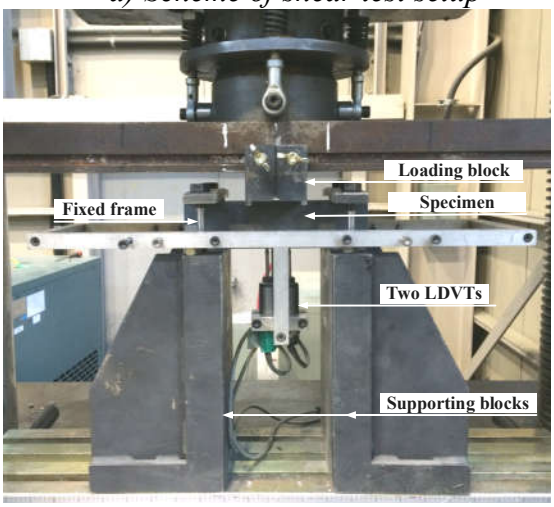

b) A prototype at Sejong University

Fig 3. Shear test setup at static rates

$$V = C.\varepsilon_f \qquad (1)$$

Where, C is the wave velocity of energy frame ($C = \sqrt{E/\rho}$), E is the elastic modulus of the energy frame, ρ is the density of the energy frame, and ε_f is the strain of the energy frame when the coupler fails.

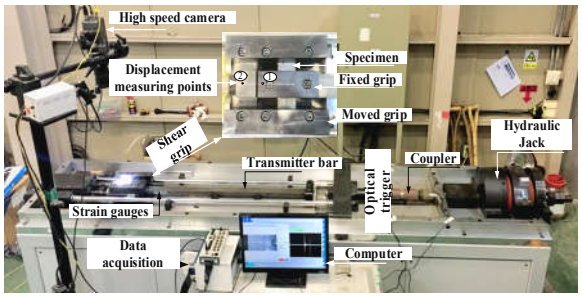

a) Prototype in Sejong University (I-SEFIM)

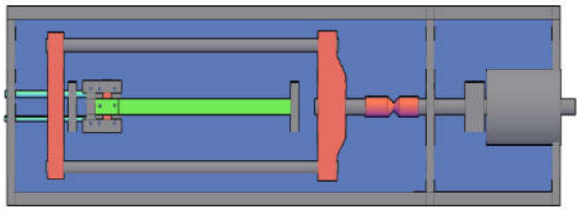

b) Model of shear impact system

Fig 4. Shear test setup at high strain rates

3. Results and discussion

Fig. 5 shows the failure of UHPFRCs specimen at static and high strain rate tests. From the test results indicated that all the specimens failed with two major diagonal shear cracks accompanied by several fine flexural-shear cracks. The dominant trend of cracks was diagonal with the longitudinal axis of the specimen at an angle of 45^0. In addition, the UHPFRC specimen at high strain rates clearly produced more cracks than those at static rates.

Static shear test

Dynamic shear test

Fig 5. Failure of shear specimens

Fig. 6 shows the average shear stress-versus-strain responses of UHPFRC reinforced with 2.0 vol.-% smooth steel fibers at different strain rates, while their average parameters were listed in Table 3. The shear stress (τ), shear strain capacity (γ), and strain rates ($\dot{\gamma}$) were calculated according to Eqs. (2) – (4) for static test and Eqs. (5) – (7) for the high rate test, respectively (Ngo & Kim, 2018), as followed:

$$\tau = \frac{P}{2bd} \quad (2)$$

$$\gamma = \frac{\delta}{a} \quad (3)$$

$$\dot{\gamma} = \frac{v}{a} = \frac{1}{60} \times \frac{1}{25} = 0.000667 \ \ s^{-1} \quad (4)$$

$$\tau = \frac{P}{2bd} = \frac{\varepsilon_{tr} \times A_{tr} \times E_{tr}}{2bd} \quad (5)$$

$$\gamma = \frac{\delta}{a} = \frac{d_2 - d_1}{a} \quad (6)$$

$$\dot{\gamma} = \frac{v_2 - v_1}{a} \quad (7)$$

where P (kN) is the applied load; δ (mm) is the displacement of the middle part of specimens; b, d, and a (mm) are the width, height, and shear span of specimens; v (mm/min) is the displacement speed of the UTM. ε_{tr}, A_{tr}, and E_{tr} are the elastic strain, cross-section area (mm^2), and elastic modulus (MPa) of the transmitter bar, respectively. d_1, v_1, d_2, and v_2 are the displacement and velocity of point 1 and point 2 on the surface of shear grip, respectively, measured by the high-speed camera system.

As can see in Table 3, shear strength (τ_{max}) and shear strain capacity (γ_{max}) of UHPFRC exhibited strong strain-rate dependent. The τ_{max} and γ_{max} at static rate were 24.4 MPa and 0.050, respectively. As the strain rate increased, the τ_{max} of UHPFRCs increased from 25.8 MPa, at the high strain rate level *h1*, to 32.0 MPa, at the strain rates level *h2*. In addition, the average value of γ_{max} increased from 0.050 at static rates to 0.057 at high strain rates level h_1 and 0.080 at high strain rates level h_2.

Table 3. Shear test results at different strain rates

Test series	Spe.	Strain rate		t_{max}	g_{max}
		Type	s^{-1}	MPa	
LS20-S	SP1	Static	$6{,}67^{-4}$	24.80	0.047
	SP2			23.38	0.054
	SP3			24.42	0.047
	SP4			25.51	0.052
	SP5			24.80	0.047
	SP6			23.38	0.054
	Average		$6{,}67^{-4}$	24.4	0.050
	SD			*0.9*	*0.003*

Test series	Spe.	Strain rate		t_{max}	g_{max}
		Type	s^{-1}	MPa	
LS20-H1	SP1	High rates h1	105	25.27	0.076
	SP2		124	26.26	0.068
	SP3		76	26.68	0.046
	SP4		119	26.20	0.027
	SP5		90	25.15	0.064
	SP6		82	25.15	0.064
	Average		99	25.8	0.057
	SD			*0.7*	*0.018*
LS20-H2	SP1	High rates h2	195	33.11	0.080
	SP2		155	31.73	0.054
	SP3		190	31.79	0.105
	SP4		185	31.87	0.088
	SP5		192	30.85	0.088
	SP6		188	32.77	0.062
	Average		184	32.0	0.080
	SD			*0.8*	*0.019*

The rate-sensitivities of UHPFRCs have been observed by previous researchers (T. K. Tran & Kim, 2012, 2014), owing to three factors including matrix, fiber, and interfacial bond strength between fiber and matrix. Among the three factors, the interfacial bond strength has been reported as a dominant factor for the high rate-sensitivity (T. K. Tran & Kim, 2013). The high rate-sensitivity of interfacial bond strength was explained as followed: at the static rates, the interfacial bond strength was originally generated by the claiming pressure of the surrounding matrix on the surface of fiber during the matrix shrinkage process (Park et al., 2014). Moreover, under the high strain rate loading, an additional pressure due to the inertial effect of the matrix surrounding fiber would increase the interfacial bond strength (T. K. Tran & Kim, 2013). It resulted in the superior UHPFRCs possibly applied in structures subjected to extreme loads.

The shear strength of UHPFRC increased as the fiber volume content increased regardless of the applied strain rates. At static rate, the τ_{max} (24.4 MPa) of UHPFRC reinforced with 2 vol.-% smooth steel fiber in this study is much higher than the 12.0 MPa and 20.3 MPa of UHPFRC reinforced with 0.5 and 1.5 vol.-% according to Ngo et al. (Ngo & Kim, 2018). A similar trend was observed at high strain rates *h1* (13.7, 20.7, and 25. 8 MPa) and *h2* (19.3, 31.4, and 32.0 MPa), as shown in Fig. 7, respectively.

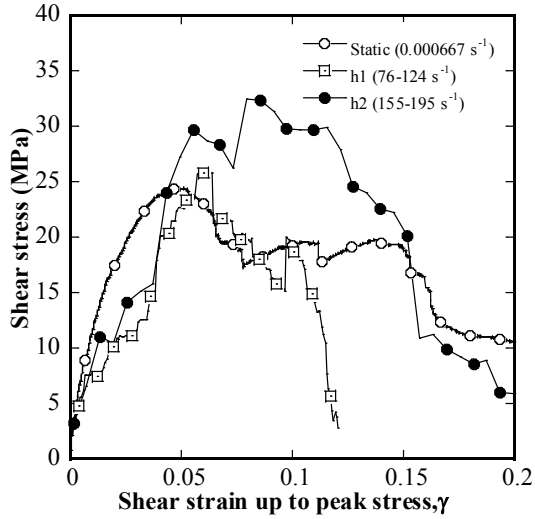

Fig 6. Shear stress versus strain response of UHPFRCs at different strain rates

The τ_{max} of investigated UHPFRCs was compared to their tensile strength (σ_{pc}), as listed in Table 4. In which, the σ_{pc} is obtained from the predicting equation proposed by (Park et al., 2016b) since there is a different strain rate level between investigated shear and tensile strain rates. As can be seen in Table 4, the τ_{max} of UHPFRC was significantly greater than the σ_{pc} at static rate. This phenomenon could be attributed to the dowel effects in addition to fiber pullout in shear (Ngo & Kim, 2018). The shear and tensile strength were obviously sensitive to the applied strain rates even though the tensile strain-rate sensitivity was higher than the shear rate-sensitivity. Specifically, the dynamic increase factor (DIF)-2.87 for the σ_{pc} was significantly greater than the DIF (1.31) for the τ_{max} at the strain rate of 184 s^{-1}. The lower rate sensitivity of τ_{max}, in comparison with the σ_{pc} of UHPFRCs, might be explained by considering lower inertial effects, in the shear specimen, of mortar matrix surrounding fibers owing to the pull-out direction of fiber: under shear failure, almost the fibers tended to align along the longitudinal axis of the specimen, which was perpendicular to the shear loading. Therefore, half of the interfacial force of the matrix surrounding fiber would result in a positive effect on the clamping pressure whereas the other half would produce a negative effect (Ngo & Kim, 2018). The correlation between shear and tensile strength (t_{max}/s_{max}) was 1.45, at static rate, decreased to 0.66 at high strain rates *h2,* owing to the lower rate-sensitivity of shear strength.

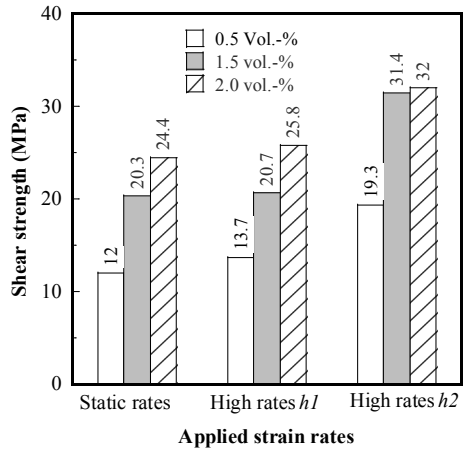

Fig 7. Effect of fiber volume content on shear strength of UHPFRCs

Table 4. Comparative tensile - shear responses

Strain rate	Shear strength, t_{max}		Tensile strength, s_{max}		t_{max}/s_{max}
s^{-1}	MPa	DIF	MPa	DIF	
0.000667	24.40	1.00	16.87	1.00	1.45
99	25.80	1.06	38.45	2.28	0.67
184	32.00	1.31	48.47	2.87	0.66

4. Conclusion

This study investigated the shear strain rate-dependent and the correlation between shear and tensile response of UHPFRCs. The following conclusions could be drawn from the limited study described herein:

- Shear and tensile strength increased as the applied strain-rates increased.
- The shear strain-rate sensitivity was not as high as the tensile strain- rate sensitivity.
- The ratios between shear and tensile strength are 1.45, 0.67, and 0.66 at static rates, high strain rates *h1*, and *h2*, respectively.

Future work should investigate the effect of various fiber parameters such as higher fiber volume content, and fiber types (hooked, twisted fiber) to observe the intensive behavior of UHPFRCs at high strain rates. In addition, the correlation of shear-flexural or tensile should be clarified to provide the input for the numerical simulation of UHPFRC structures resistant to blast and impact loading.

References

J.J. Park, S.T. Kang, K.T. Koh, S. W. K. (n.d.). *Influence of the ingredients on the compressive strength of UHPC as a fundamental study to optimize the mixing proportion.* Second International Symposium on Ultra High Performance Concrete, 105–112.

Micallef, K., Sagaseta, J., Fernández Ruiz, M., & Muttoni, A. (2014). *Assessing punching shear failure in reinforced concrete flat slabs subjected to localised impact loading*. International Journal of Impact Engineering, 71, 17–33. https://doi.org/10.1016/ j.ijimpeng.2014.04.003

Millard, S. G., Molyneaux, T. C. K., Barnett, S. J., & Gao, X. (2010). *Dynamic enhancement of blast-resistant ultra high performance fibre-reinforced concrete under flexural and shear loading*. International Journal of Impact Engineering, 37(4), 405–413. https://doi.org/10.1016/ j.ijimpeng.2009.09.004

Millon, O., Riedel, W., Thoma, K., Fehling, E., & Nöldgen, M. (2009). *Fiber-reinforced ultra-high performance concrete under tensile loads.* DYMAT 2009 - 9th International Conferences on the Mechanical and Physical Behaviour of Materials under Dynamic Loading, 1, 671–677. https://doi.org/10.1051/dymat/2009095

Ngo, T. T., & Kim, D. J. (2018). *Shear stress versus strain responses of ultra-high- performance fiber-reinforced concretes at high strain rates*. International Journal of Impact Engineering, 187–198. https://doi.org/https://doi.org/10.1016/j.ijimpeng. 2017.09.010

Ngo, T. T., Park, J. K., & Kim, D. J. (2019). *Loading rate effect on crack velocity in ultra-high-performance fiber-reinforced concrete*. Construction and Building Materials, 197(2019), 548–558. https://doi.org/ 10.1016/j.conbuildmat.2018.11.241

Ngo, T. T., Park, J. K., Pyo, S., & Kim, D. J. (2017). *Shear resistance of ultra-high-performance fiber-reinforced concrete*. Construction and Building Materials, 151, 246–257. https://doi.org/ 10.1016/j. conbuildmat.2017.06.079

Park, S. H., Kim, D. J., & Kim, S. W. (2016a). *Investigating the impact resistance of ultra-high-performance fiber-reinforced concrete using an improved strain energy impact test machine.* Construction and Building Materials, 125, 145–159. https://doi.org/10.1016/ j.conbuildmat. 2016.08.027

Park, S. H., Kim, D. J., & Kim, S. W. (2016b). *Investigating the impact resistance of ultra-high-performance fiber-reinforced concrete using an improved strain energy impact test machine.* Construction and Building Materials, 125, 145–159. https://doi.org/ 10.1016/j.conbuildmat. 2016.08.027

Park, S. H., Ryu, G. S., Koh, K. T., & Kim, D. J. (2014). *Effect of shrinkage reducing agent on pullout resistance of high-strength steel fibers embedded in ultra-high-performance concrete*. Cement and Concrete Composites, 49, 59–69. https://doi.org/10.1016/j. cemconcomp.2013.12.012

Thai, D., & Kim, S. (2014). *Failure analysis of reinforced concrete walls under impact loading using the finite element approach*. ENGINEERING FAILURE ANALYSIS, 45, 252–277. https://doi.org/10.1016/j. engfailanal. 2014.06.006

Tran, N. T., Tran, T. K., Jeon, J. K., Park, J. K., & Kim, D. J. (2016). *Fracture energy of ultra-high-performance fiber-reinforced concrete at high strain rates.* Cement and Concrete Research, 79, 169–184. https://doi.org/10.1016/j.cemconres.2015.09.011

Tran, T. K., & Kim, D. J. (2012). *Strain energy frame impact machine (SEFIM).* Journal of Advanced Concrete Technology, 10(3), 126–136. https://doi.org/10.3151/jact.10.126

Tran, T. K., & Kim, D. J. (2013). *Investigating direct tensile behavior of high performance fiber reinforced cementitious composites at high strain rates.* Cement and Concrete Research, 50, 62–73. https://doi.org/10.1016/j.cemconres.2013.03.018

Tran, T. K., & Kim, D. J. (2014). *High strain rate effects on direct tensile behavior of high performance fiber reinforced cementitious composites.* Cement and Concrete Composites, 45, 186–200. https://doi.org/10.1016/ j.cemconcomp.2013.10.005

Wu, Z., Shi, C., He, W., & Wang, D. (2017). *Static and dynamic compressive properties of ultra-high performance concrete (UHPC) with hybrid steel fiber reinforcements.* Cement and Concrete Composites, 79. https://doi.org/10.1016/ j.cemconcomp.2017.02.010